3-1-2014

Stochastic Real-time Optimal Control for Bearing-only Trajectory Planning

Steven M. Ross

Richard G. Cobb
Air Force Institute of Technology

William P. Baker
Air Force Institute of Technology

Stochastic Real-Time Optimal Control for Bearing-Only Trajectory Planning

Steven M. Ross[1], Richard G. Cobb[2], and William P. Baker[3]
Air Force Institute of Technology, Wright-Patterson Air Force Base, Ohio 45433
[1]Commander, 586th Flight Test Squadron, Holloman AFB, NM 88330; steven.ross.1@us.af.mil
[2]Associate Professor, Department of Aeronautics and Astronautics; richard.cobb@afit.edu
[3]Associate Professor, Department of Mathematics and Statistics; william.baker@afit.edu

ABSTRACT

A method is presented to simultaneously solve the optimal control problem and the optimal estimation problem for a bearing-only sensor. For bearing-only systems that require a minimum level of certainty in position relative to a source for mission accomplishment, some amount of maneuver is required to measure range. Traditional methods of trajectory optimization and optimal estimation minimize an information metric. This paper proposes constraining the final value of the information states with known time propagation dynamics relative to a given trajectory which allows for attainment of the required level of information with minimal deviation from a general performance index that can be tailored to a specific vehicle. The proposed method does not suffer from compression of the information metric into a scalar, and provides a route that will attain a *particular* target estimate quality while maneuvering to a desired relative point or set. An algorithm is created to apply the method in real-time, iteratively estimating target position with an Unscented Kalman Filter and updating the trajectory with an efficient pseudospectral method. Methods and tools required for hardware implementation are presented that apply to any real-time optimal control (RTOC) system. The algorithm is validated with both simulation and flight test, autonomously landing a quadrotor on a wire.

NOMENCLATURE

$\mathbf{C}$	=	path constraints
f	=	dynamics function
$\mathbf{h}$	=	measurement function
$\mathbf{H}$	=	Jacobian of measurement function
$\mathcal{I}$	=	Fisher Information Matrix
J	=	cost functional
$\mathcal{L}$	=	Lagrange cost functional
$\mathbf{P}$	=	covariance matrix (m^2)
P_{xx}, P_{zz}	=	directional covariance elements (m^2)
$\mathbf{R}$	=	sensor uncertainty (deg^2)
t	=	time (sec)
x, y, z	=	Cartesian coordinates (m)
$\mathbf{u}$	=	control vector (m/s^2)
$\mathbf{v}$	=	velocity vector (m/s)
W	=	weighting factor
$\mathbf{W_u}$	=	control weighting matrix
$\mathbf{x}$	=	camera coordinates in navigation frame (m)
$\mathbf{x}_k$	=	path planner state history, solved at epoch k
$\tilde{\mathbf{x}}$	=	augmented state vector
$\mathbf{z}$	=	measurement vector (deg)
α	=	gain on sigma-point spread
β	=	angle to target (deg)

Γ	=	Mayer cost functional
γ	=	boundary conditions
Δt	=	time step (s)
Δt_{calc}	=	combined loop time for optimization, estimation, and communication (s)
Δt_{meas}	=	measurement time interval (s)
ζ_i	=	information state
η	=	measurement noise
k	=	UKF tuning parameter
λ	=	UKF scaling factor
$\Xi_{a\to b}$, Ξ_{corr}	=	cosine vector from a to b, cosine correction matrix
ρ	=	range to target (m)
σ	=	standard deviation
$\Phi_{k+1\|k}$	=	transition matrix, time t_k to t_{k+1}
$\mathbf{X}$	=	sigma-point matrix
Ω	=	time span (s)

Subscripts

0	=	initial
app	=	at approach point, the final state of approach segment
bl	=	blending time
c	=	covariance
f	=	final
k	=	time step or path planner epoch
m	=	mean
perch	=	at landing point
r	=	relative
t	=	target
x, y, z	=	direction component

Superscripts

*	=	optimal
^	=	estimated parameter
-, +	=	pre/post measurement update

1. INTRODUCTION

Bearing-only tracking is a classical navigation problem. Many real-world systems depend on angle-only sensors for target state estimation, such as submarines using only passive sonar, high-speed anti-radiation missiles (HARM), robots, and unmanned aerial vehicles (UAVs) using images from an optical sensor. The inability to sense range with each measurement, combined with the inherent nonlinearity of the problem make estimation of a target's location and motion problematic. Moving the sensor orthogonal to the line-of-sight (LOS) generates observability for range estimation, and many researchers have pursued optimal methods for trajectory planning in this context [1-6]. Optimal trajectory planning of any sort, however, is notoriously difficult to implement for on-line systems (excepting those simple enough to have a closed-form analytical feedback solution). Notably, recent advances in direct optimization through techniques such as pseudospectral methods (PSM) [7-9] have increased the efficiency and stability of obtaining a numeric optimal solution to the point where real-time optimal control (RTOC) of systems with moderate speed dynamics is now possible.

This paper proposes a new method of approaching the bearing-only trajectory planning problem that enables simultaneous consideration of both the optimal control problem and a system's prescribed final estimation requirements, overcoming the typical limitations of previous approaches which address each requirement separately. The trajectory planning goal is to provide an optimal trajectory for arrival at a point, or set of points, potentially offset from a relative target position, the location of which must be determined to a predefined certainty by varying the engagement geometry along the way. Instead of driving the shape of the trajectory with minimization of an optimization metric, a general performance index (not necessarily related to information) is allowed, tailored to the observer vehicle. No change in a "perfect knowledge" optimal course is made unless the planned route is not expected to attain the

amount of observability required for accomplishment of tasks such as landing or weapons employment, optimally considering the stochastic nature of the expected future measurements. In this case, the original optimal course is modified to achieve the future objectives, and is updated as more target information becomes available.

Consideration of noise and disturbances mandate the need for the trajectory planning capability to be part of an on-line system, made fast and simple enough to be applied recursively with an estimation filter using position feedback and new measurement data. The goal of the research was to design the complete guidance system, and apply it to a UAV power line landing scenario, addressing the real-world issues that occur when RTOC is taken beyond simulation. Verification of the system was performed through flights test of a quadrotor that was guided to a wire and landed upon it, for the intent of energy harvesting to extend range and station time.

1.1. Trajectory Optimization for Bearing-only Tracking

Trajectory modification for the purpose of bearing-only tracking (BOT), or localization (static target), has been heuristically implemented in the submarine community for at least 60 years [10]. Most efforts to increase the efficacy of the observer's trajectory on target state estimation have attempted to optimize a path based on control from two general categories—pure localization, and "dual control theory," a hybrid of estimation and control. For pure localization, the trajectory is optimized for the best possible target position estimate given a set of vehicle dynamics and a prescribed amount of time. The performance index reflects the amount of information gathered by the sensor along a path, and some measure of the Fisher Information is most commonly used. The Fisher Information is defined as the variance of the score of a likelihood function (the probability density of the set of measurements conditioned on the set of states), where E is the expected value, and can be found as a byproduct of the development of the Cramér-Rao Lower Bound (CRLB) in [11] :

$$\mathcal{I}_k = E\left[\left(\frac{\partial}{\partial \mathbf{x}_k}\ln p_{\mathbf{z}_k|\mathbf{x}_k}\right)^2\middle|\mathbf{x}_k\right] \tag{1}$$

The Fisher Information Matrix (FIM) can be shown to be the observability Grammian for the linear case [12]. It is a function of observability from the geometry of the problem, rather than the estimation method. For the submarine passive sonar context, the basic framework is set up in [4], and expanded on in [13]. To form a suitable localization performance index, the directional information in the matrix must be compressed into a scalar value upon which to optimize. Maximization of the determinant of the FIM, a determinant lower bound, or a determinant approximation [2, 5, 6, 14-16] effectively minimizes the volume of the uncertainty ellipsoid around the target estimate, but highly eccentric ellipsoid shapes can result [17]. Similar options (sometimes only semantically different) include the trace of the CRLB [18], the trace of the covariance matrix [3], maximization of the smallest FIM eigenvalue [19], minimization of the trace of the inverse of the FIM [20], or minimization of the differential entropy of the posterior target density (equivalent to maximizing the FIM determinant for the Gaussian case) [21].

The citations above are not exhaustive, but common drawbacks for all localization methods include the aforementioned loss of directional information when compressing the information metric to a scalar cost function, and a major limitation of requiring prescription of an arbitrary final time. This is often accomplished indirectly, through methods such as prescribing the final travel distance of a constant speed observer, or prescribing the number of final time measurements gained at a constant interval. The optimal trajectory is highly sensitive to the horizon selected [5, 14, 21], making the optimality of the solution more of a mathematical construct than a practical reality. Finally, the purpose of localization is to produce the best target location estimate—the actual path is of no consequence, save obeying system dynamics and being restricted from collision with the target (the optimal method of increasing information—this is prevented by limiting the final time for submarines or using a fixed altitude for the case of a UAV above a target).

1.2. The Dual Control Problem

Dual control or *dual effects* theory [22] adds consideration of a primary mission to localization efforts. The two purposes may directly conflict, but both are necessary. In full form, the problem is by definition nonholonomic—the final state (in terms of target certainty) is a function of the path taken to achieve it. As such, the control and estimation concepts are fundamentally coupled and *inseparable* [23]—the quality of estimation affects the quality of control and vice versa [24]. Dynamic programming and search-based approaches are the general solution techniques, but are commonly prohibitive even for small problems [25-27].

Several different approaches to solving the dual control problem have been proposed to make the problem more tractable. Geometric considerations on estimation have been removed by focusing simply on "camera-on-target" time or homing, and solved with several methods, such as direct collocation [28, 29], neural networks [30], or heuristics [31-33]. Others have reduced the problem to one physical dimension, usually mandating a constant closure to a target and controlling in an orthogonal dimension with pure localization [34, 35]. Weighting schemes have been proposed to balance non-information related control (e.g. LQR) to some centerline and a "nudge" factor to drive the system away from the centerline in an effort to increase observability based on current target position uncertainty [24, 36-38]. Analytical solutions can sometimes be found for an optimal next step with a *one-step-ahead* method, assuming the next measurement will be the last [3, 24, 39]. While in a sense more optimal, taking the optimal next step does not necessarily achieve the optimal path overall. It was found that choosing more than one or two steps ahead was not practically implementable in real-time [40].

This paper seeks to address some of the limitations of the previous methods by changing the fundamental approach to the dual control problem. The reoccurring theme in the aforementioned research approaches is the presence of a scalar information metric in the performance index. The proposed method however embeds the information requirements of the mission within the constraints. The performance index is then free to be set to meet the primary mission needs. No directional information is lost in compression. No final time horizon or fixed vehicle speeds need to be set, freeing the solution trajectory to increase or decrease in length or duration, allowing the observer to slow down and "dwell" for more measurements when the line-of-sight to the target is particularly valuable. Most importantly, the projected trajectory will meet the true requirements of many bearing-only systems that need a particular minimum amount of final target certainty to accomplish their mission (to fire a torpedo, to hit a target, to land on a power line, etc.) based on the physical system realities. Previous methods only deliver "more" or "less" certainty. The exception would be Frew, who did project to a final certainty with an exhaustive search approach [25].

2. PROBLEM DESCRIPTION

Consider the autonomous control of small UAVs for surveillance and other related missions. The scope of this paper addresses a small part of the overall mission—energy harvesting from a power line. Short range and limited station times are active constraints on the usefulness of our current small and micro-UAVs. Both could be greatly extended through the ability to recharge batteries through induction. The technology has become commonplace with mats for cordless devices and such, and application to UAVs is a current research effort at Defense Research Associates (DRA). In addition to increasing range, a small group of UAVs could be sent for surveillance of the same target. Conceptually, with two observers recharging on a nearby power line and a third in the air, continuous coverage could be provided without operator input.

The control process for landing on a power line will require several mode switches, including an *acquisition segment*, where control is provided to reach a position for likely power line detection. This is followed by an *approach segment*, where control is determined to an offset approach point while considering the observability needs for accurate estimation of that point. Finally, control in the *flare segment* is provided to maneuver from the given offset in a manner that will safely attach to the wire. The concept is demonstrated in Figure 1.

The acquisition segment is within our current capability. It is assumed that the vehicle has a rough knowledge of power line locations from local maps or imagery and sufficient navigation capacity to avoid terrain and maneuver orthogonal to the wire through GPS, INS, optical flow, or some other indigenous system. Identification can be accomplished with a line detection algorithm operating on images collected from a common small UAV sensor such as a webcam.

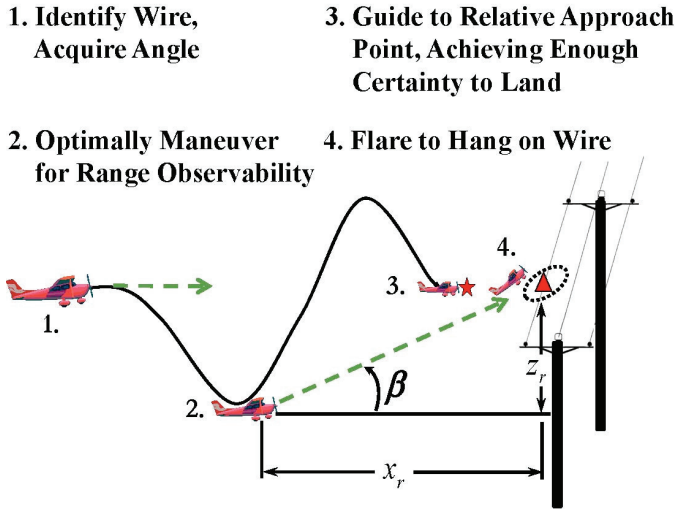

Figure 1. Conceptual Approach and Flare Segments

This paper addresses the approach segment—beginning with an initial measurement of approach angle (pitch) to the wire, and ending at an approach point with the required system state to begin the flare segment. The approach point is defined relative to the wire's true location, which must be estimated to a defined final certainty prior to arrival based on the actual size of the hook to attach to the wire and the mean-squared position error in the vehicle's ability to attain a commanded point. The flare segment is currently being investigated by several institutions for fixed-wing UAVs. In [41], a fixed-wing glider was perched on a wire using an aggressive flare maneuver from both 2.5 m and 1.5 m approach points, using full information about the location of the wire. The approach point in this work, x_{app}, was correspondingly set to 2 m.

The test platform for the algorithm was a quadrotor with the ability to hover, so an aggressive flare segment at the end of the trajectory was not required as would be for a fixed-wing UAV. Thus, the final condition in the optimal controller was set to achieve minimum estimation certainty in the position of the approach point and to slow to a hover there. The RTOC control mode is then switched off, and the quadrotor flies directly to the last known location of the wire, gently slowing to a stop and lowering itself to engage a hook on top of the vehicle.

3. MODELING

To focus on the RTOC application, all details concerning IMU, body, controller, camera, and Vicon frames and transformations, Euler orientation angles and rates, filtering for own-ship position, inner and mid-level control loops, and image processing are omitted. It is assumed that a delayed, noise corrupted measurement angle to the wire is available from a sensor in front of the craft using a line detection algorithm. The angle is corrected to vertical with pitch and roll angles, and lateral motion along the wire is not observable. With no observable lateral changes, there is no benefit to flight parallel to the wire, and the optimal min-time solution becomes planar (2-D), maneuvering vertically only to increase observability.

A local, planar navigation frame is defined with coordinates of the camera relative to an inertial point, $\mathbf{x} \in R^2$:

$$\mathbf{x} = \begin{bmatrix} x & z \end{bmatrix}^{\mathrm{T}} \tag{2}$$

Velocity is simply:

$$\mathbf{v} = \begin{bmatrix} v_x \\ v_z \end{bmatrix} = \frac{d\mathbf{x}}{dt} \tag{3}$$

An upper total velocity limit, $v_x^2 + v_z^2 \le v_{max}^2$, was imposed (no minimum speed is required for a quadrotor), but in the manner controls were actually applied to the quadrotor for flight test, individual limitations of $|v_x| \le v_{xmax}$, $|v_z| \le v_{zmax}$ became more restrictive and were imposed as safety constraints only. For notational convenience, relative coordinates between the target and the vehicle are defined as:

$$\mathbf{x}_r \equiv \begin{bmatrix} x_r \\ z_r \end{bmatrix} = \begin{bmatrix} x_t - x \\ z_t - z \end{bmatrix} \tag{4}$$

The measurement function is nonlinear, and a discrete measurement, z_k, is modeled as an independent Gaussian random variable:

$$z_k = \hat{\beta}_k = \mathbf{h}(\mathbf{x}_k) + \eta_k \tag{5}$$

with $E[\eta_k] = 0$ and $E[\eta_k, \eta_j^T] = \mathbf{R}\delta_{kj}$, for a constant variance between measurements. The true measurement is the vertical angle from inertial level at the sensor to the target ($\tan^{-1}$ refers to the full quadrant arctangent):

$$\mathbf{h}(\mathbf{x}) \equiv \beta = \tan^{-1}\left(z_r / x_r\right) \tag{6}$$

Control for the quadrotor, $\mathbf{u} \in R^2$, can be decoupled into direct acceleration in the vertical and horizontal axes:

$$\mathbf{u} = \begin{bmatrix} u_x \\ u_z \end{bmatrix} = \frac{d\mathbf{v}}{dt} \tag{7}$$

limited by $|u_x| \le \left(\frac{dv_x}{dt}\right)_{max}$ and $\left(\frac{dv_z}{dt}\right)_{min} \le u_z \le \left(\frac{dv_z}{dt}\right)_{max}$, with gravity potentially causing a difference in vertical acceleration capability. For outer-loop trajectory planning, this was found to be sufficient.

For actual propagation and use in the own-ship position Kalman Filter, the discrete-time state equation was used:

$$\mathbf{x}_{k+1}^{(KF)} \equiv \begin{bmatrix} x_{k+1} \\ z_{k+1} \\ v_{x_{k+1}} \\ v_{z_{k+1}} \end{bmatrix} = \begin{bmatrix} \mathbf{I}_2 & \mathbf{I}_2\Delta t \\ \mathbf{0}_2 & \mathbf{I}_2 \end{bmatrix} \mathbf{x}_k^{(KF)} + \begin{bmatrix} \mathbf{0}_2 \\ \mathbf{I}_2\Delta t \end{bmatrix} \mathbf{u}_k + \boldsymbol{w}_k \tag{8}$$

with $E[\boldsymbol{w}_k] = 0$ and $E[\boldsymbol{w}_k \boldsymbol{w}_i^T] = \mathbf{Q}_k\delta_{ik}$.

3.1. Information States

Control is desired to efficiently take the vehicle to an approach point defined relative to the wire while acquiring the required certainty in the wire's position, without artificial limits on time, the number of measurements, or similar constraints. An elegant, single-shot solution (as opposed to solving the dual control problem with arbitrary weights, and iteratively adjusting the weights) is desired that will guarantee the final minimum covariance is met in each direction without wasting additional maneuver effort. In order to apply this condition as a constraint directly, a state (or combination of states) must be created to encapsulate the final covariance of the system. This requires an expression for how the covariance, dependent on discrete measurement updates and geometrical principles, changes with respect to time. The continuous Kalman Filter equations assume a continuously available measurement and result in a sluggish, inaccurate estimate for systems such as this with a low update rate (2-3 Hz). The EKF update equations can be used to form an approximation, but the result involves not only

linearization at each time step (vice measurement point), but multiple matrix multiplications and an inverse. The method is poorly conditioned and leads to numeric instabilities. Propagation of the inverse covariance, however, can be more readily accomplished. With the worst-case assumption of zero initial information, this becomes the Fisher Information Matrix.

With the assumption that the vehicle's own-ship position certainty has reached steady state, the relative position problem requires no process noise to inflate the covariance between measurements. The additional relative position uncertainty can then be expressed with discrete updates of the FIM from Eq. (1), put into recursive form [42]. Linearizing about each measurement point, the matrix is rotated to the current direction and the new information is added:

$$\mathcal{I}_{k+1|k} = \left[\boldsymbol{\Phi}_{k+1,k}^{\mathrm{T}}\right]^{-1} \mathcal{I}_k \boldsymbol{\Phi}_{k+1,k}^{-1} + \mathbf{H}_{k+1}^{\mathrm{T}} \mathbf{R}_{k+1}^{-1} \mathbf{H}_{k+1} \tag{9}$$

As the root of the Kalman Filter, a pure least squares approach will produce an equivalent equation. For the Cartesian coordinate system, the transition matrix from update time t_k to t_{k+1}, $\boldsymbol{\Phi}_{k+1,k}$, becomes the identity matrix, as no rotation is necessary if the target estimate coordinates are anchored to the navigation frame. This greatly simplifies the process of estimating the information states. The Jacobian of the measurement model contains the information necessary to determine the value of each new measurement, namely the direction it was taken from and the range, $\rho_k = \sqrt{x_{r_k}^2 + y_{r_k}^2}$:

$$\mathbf{H}_k \equiv \nabla_{\mathbf{x}_k} \mathbf{h}(\mathbf{x}_k) = \begin{bmatrix} \dfrac{z_{r_k}}{\rho_k^2} & \dfrac{-x_{r_k}}{\rho_k^2} \end{bmatrix} \tag{10}$$

An optional amount of *a priori* information based on the problem setup, $\mathbf{I}_0$, is assumed, as is a constant sensor variance, $\mathbf{R} = \sigma_\beta^2$. With the appropriate trigonometric identities applied to Eq. (9) and Eq. (10), the entire information history becomes:

$$\mathcal{I}_k = \mathcal{I}_0 + \frac{1}{\sigma_\beta^2} \begin{bmatrix} \displaystyle\sum_{i=1}^{k} \frac{\sin^2 \beta_i}{\rho_i^2} & -\displaystyle\sum_{i=1}^{k} \frac{\sin \beta_i \cos \beta_i}{\rho_i^2} \\ -\displaystyle\sum_{i=1}^{k} \frac{\sin \beta_i \cos \beta_i}{\rho_i^2} & \displaystyle\sum_{i=1}^{k} \frac{\cos^2 \beta_i}{\rho_i^2} \end{bmatrix} \tag{11}$$

This form is the most intuitive, as a simple inspection shows that the quality of information about the target position in each axis (the diagonals) that is gained from each measurement is a function of how orthogonal the measurement was to that axis, and how close the sensor was to the target. Compressing this matrix into a determinant, trace, or other scalar value loses the directional quality available here that provides the path planning system with not only the amount of information still needed in each axis, but where to go to get it. Note that the diagonal elements of the information matrix don't directly translate into a level of certainty. The covariance matrix elements are instead desired, incorporating the information cross-correlation terms. From the definition of the CRLB, an efficient estimator has the property $\mathbf{I}_k = \mathbf{P}_k^{-1}$, so the covariance is easily attainable given the FIM elements. The goal, therefore, is to develop a method to constrain the final covariance in the context of the optimal control problem, and this will be done through the propagation of "information states." A constant measurement rate is assumed, Δt_{meas}, and an integral is used to approximate the summation:

$$\mathcal{I}_k \approx \mathcal{I}\left(t=t_k\right) \equiv \mathcal{I}_0 + \begin{bmatrix} \int_{t_0}^{t_k} \frac{\sin^2\beta(t)}{\Delta t_{meas}\sigma_\beta^2\rho^2(t)}\,dt & -\int_{t_0}^{t_k} \frac{\sin\beta(t)\cos\beta(t)}{\Delta t_{meas}\sigma_\beta^2\rho^2(t)}\,dt \\ -\int_{t_0}^{t_k} \frac{\sin\beta(t)\cos\beta(t)}{\Delta t_{meas}\sigma_\beta^2\rho^2(t)}\,dt & \int_{t_0}^{t_k} \frac{\cos^2\beta(t)}{\Delta t_{meas}\sigma_\beta^2\rho^2(t)}\,dt \end{bmatrix}$$
$$\equiv \mathcal{I}_0 + \begin{bmatrix} \int_{t_0}^{t_k} \dot{\zeta}_1(t)\,dt & \int_{t_0}^{t_k} \dot{\zeta}_3(t)\,dt \\ \int_{t_0}^{t_k} \dot{\zeta}_3(t)\,dt & \int_{t_0}^{t_k} \dot{\zeta}_2(t)\,dt \end{bmatrix} \tag{12}$$

Information states, $\zeta_i(t)$, are then defined with the appropriate element of for an initial condition, and propagated with the dynamics:

$$\frac{d\mathcal{I}(t)}{dt} = \begin{bmatrix} \dot{\zeta}_1(t) & \dot{\zeta}_3(t) \\ \dot{\zeta}_3(t) & \dot{\zeta}_2(t) \end{bmatrix} \tag{13}$$

Figure 2 shows the results of taking a known trajectory (from flight test Run #1) and calculating the discrete covariance elements from EKF equations alongside the continuous values obtained by propagating the information states along the same trajectory, and inverting the resulting FIM.

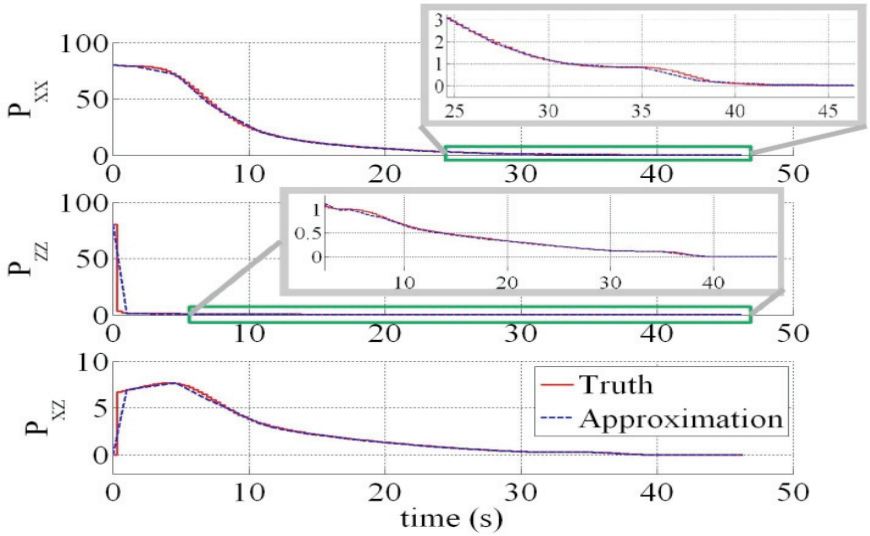

Figure 2. Comparison of EKF Covariance with Elements of the Inverse of the Information Matrix Approximation.

4. THE OPTIMAL CONTROL AND ESTIMATION PROBLEM

The optimal control problem can now be formulated using an augmented state vector:

$$\tilde{\mathbf{x}} = \begin{bmatrix} x & z & v_x & v_z & \zeta_1 & \zeta_2 & \zeta_3 \end{bmatrix}^{\mathrm{T}} \tag{14}$$

Control is defined in Eq. (7). In Bolza form, the optimal control problem is to determine the state-control function pair, $\{\tilde{\mathbf{x}}(t), \mathbf{u}(t)\}$, and final time, t_f (t_0 is known for each epoch), which minimize the cost functional:

$$J = \Gamma\left(\tilde{\mathbf{x}}\left(t_0\right), t_0, \tilde{\mathbf{x}}\left(t_f\right), t_f\right) + \int_{t_0}^{t_f} \mathcal{L}\left(\tilde{\mathbf{x}}\left(t\right), \mathbf{u}\left(t\right), t\right) dt \tag{15}$$

subject to the dynamic constraints:

$$d\tilde{\mathbf{x}}/dt = \boldsymbol{f}\left(\tilde{\mathbf{x}}(t), \mathbf{u}(t), t\right) \tag{16}$$

the path constraints:

$$\mathbf{C}\left(\tilde{\mathbf{x}}(t), \mathbf{u}(t), t_0, t_f\right) \leq \mathbf{0} \tag{17}$$

and the boundary conditions:

$$\boldsymbol{\gamma}\left(\tilde{\mathbf{x}}(t_0), t_0, \tilde{\mathbf{x}}(t_f), t_f\right) \leq \mathbf{0} \tag{18}$$

with equality constraints imposed via a second constraint on the additive inverse.

One advantage of incorporating final covariance as a boundary constraint in the optimal control problem is that any performance index can be used that best fits the situation. For the UAV scenario seeking a quick path to the approach point, the final time should be minimal, $\Gamma = t_f$. A small quadratic cost on control, $\mathcal{L} = \mathbf{u}^{\mathrm{T}}\mathbf{W}_u\mathbf{u}$, is added to ensure a smooth flight trajectory and to avoid any issues with a singular arc resulting from having no control terms with which to minimize the Hamiltonian. The weights in $\mathbf{W}_u$ were (arbitrarily) set to 0.1 on each diagonal element to make a very small contribution, and no Lagrange penalty is set for the states, which should be free to maneuver to any value necessary within the limitations of $\mathbf{C}$. Weighting could easily be added in other applications for best possible tracking, or avoidance of areas while still gaining the required certainty for mission accomplishment.

4.1. Constraints

Dynamic constraints, $\boldsymbol{f}$, were added as shown in Eqs. (3), (7), and (13). Path constraints scaled the problem, reducing the physical limitations to fit inside the available indoor flight test facility in order to make use of a Vicon motion capture system. In practice, the optimization software used required inequality constraints on all states and controls. Variables not intended to be constrained had values set well out of a realistic range, but not set at infinity to keep gradients meaningful. The potentially active constraints of $\mathbf{C}$ are shown in a consolidated notation:

$$\begin{bmatrix} -9\ \mathrm{m} \\ 0.8\ \mathrm{m} \\ -0.5\ \mathrm{m/s} \\ -0.5\ \mathrm{m/s^2} \\ -30^\circ \end{bmatrix} \leq \begin{bmatrix} x \\ z \\ v_x, v_z \\ u_x, u_z \\ \beta \end{bmatrix} \leq \begin{bmatrix} x_{app\_offset} + \hat{x}_t \\ 5.5\ \mathrm{m} \\ 0.5\ \mathrm{m/s} \\ 0.5\ \mathrm{m/s^2} \\ 40^\circ \end{bmatrix} \tag{19}$$

The forward component, x, was limited to stay between the approach point, $x_{app} = x_{app\_offset} + \hat{x}_t$, and the wall of the flight facility furthest from it (where the run was started). The approach point itself is only an estimate, changing each epoch, but it does provide some safety buffer until the desired target certainty is reached. Vertical limits were set so that the landing gear would remain clear of the floor and a "ceiling" limit ensured that the vehicle would stay low enough for reception by a sufficient number of Vicon cameras. In a real power line landing scenario, the upper limit could be removed (assuming no airspace limitations), simplifying the problem for the optimal solver, and the "ground" limit could be replaced with a minimum-safe-altitude function from a terrain model. For this indoor flight, the vehicle speed was limited to increase the flight time, making the total engagement representative of an actual approach, and allowing for a realistic test of the ability of the RTOC system to control in real-time despite the inherent computational delays. The path constraint on β was based on the estimated target position, intended to keep the vehicle in a position for the fixed camera to maintain the wire within the field-of-view (FOV). No measurements are received when outside the true

FOV. This is always the case as the vehicle transitions to land-mode and flies underneath the wire, but could potentially happen during the flight due to disturbances or a bad target estimate.

4.2. Boundary Conditions

The solution of the optimal control problem is iterative. The initial conditions for each epoch are not the current conditions, but the intended *future* conditions at the time the next solution is expected to become available. A complete loop time, Δt_{calc}=0.9 sec, is assumed inclusively for the optimization problem, the estimation problem, and all transport delays (based on experience with the current hardware). The very first solution is seeded with the current position at a hover. After one optimal trajectory exists, position and velocity initial conditions are taken from the previous epoch's solution, $\hat{x}_k(t)$, propagated forward by Δt_{calc} :

$$\begin{bmatrix} \mathbf{x}_{0_{k+1}} & \mathbf{v}_{0_{k+1}} \end{bmatrix}^{\mathrm{T}} = \begin{bmatrix} \mathbf{x}_k(t+\Delta t_{calc}) & \mathbf{v}_k & (t+\Delta t_{calc}) \end{bmatrix}^{\mathrm{T}} \tag{20}$$

The information states are only estimates of the true FIM components, based on future assumed measurements consistently received at a fixed time interval. The realities of processing delays, poor image backgrounds, and hardware malfunctions in general lead occasionally to slow or skipped measurements, and the accuracy of the information state estimates will drift over time. Initial conditions are therefore reset at each epoch based on an inverse of the actual covariance from the estimation filter, $\mathbf{P}_k$, propagated forward on the optimal path by Δt_{calc}. As measurement times may vary, an expected measurement time vector is created based on the actual reception time of the last measurement, t_{last_meas}:

$$t_{meas} = [t_{last\_meas} + \Delta t_{meas}, t_{last\_meas} + 2\Delta t_{meas}, \ldots, t_{last\_meas} + n\Delta t_{meas}] \tag{21}$$

where n represents the maximum number of measurements that can be incorporated such that:

$$t_{last\_meas} + n\Delta t_{meas} \le t_k + \Delta t_{calc} = t_{0_{k+1}} \tag{22}$$

The measurement Jacobian is calculated by solving for the expected relative state vector at each of these times and applying Eq. (10). The expected covariance is found by applying the recursive form of the EKF equation for each of the measurements to be considered:

$$\mathbf{P}_{i+1} = \mathbf{P}_i - \mathbf{P}_i \mathbf{H}_i^{\mathrm{T}} \left(\mathbf{H}_i \mathbf{P}_i \mathbf{H}_i^{\mathrm{T}} + \mathbf{R} \right)^{-1} \mathbf{H}_i \mathbf{P}_i \tag{23}$$

The result is $\mathbf{P}_{0k+1} = \mathcal{I}^{-1}_{0k+1}$, and the elements of the inverse are used as the initial conditions for each of the information states.

The final conditions in γ for the first four states take the system to a hover at the approach point:

$$\begin{bmatrix} x_{k+1}(t_f) \\ z_{k+1}(t_f) \\ v_{x_{k+1}}(t_f) \\ v_{z_{k+1}}(t_f) \end{bmatrix} = \begin{bmatrix} x_{app\_offset} + \hat{x}_k \\ z_{app\_offset} + \hat{z}_k \\ 0 \\ 0 \end{bmatrix} \tag{24}$$

The required covariance for mission accomplishment is applied in the boundary conditions for the information states. The physical considerations of the hook size (used to "land" on the wire), in addition to the steady-state uncertainty of the vehicle's own-ship position estimate determine $P_{xx_{max}}$ and $P_{zz_{max}}$, the required diagonal elements of the covariance matrix. The elements can be found from the

information states with simple inverse relationships:

$$\begin{aligned} P_{xx}(t_f) &= \zeta_2(t_f) \Big/ \left[\zeta_1(t_f)\zeta_2(t_f) - \zeta_3^2(t_f)\right] \le P_{xx_{max}} \\ P_{zz}(t_f) &= \zeta_1(t_f) \Big/ \left[\zeta_1(t_f)\zeta_2(t_f) - \zeta_3^2(t_f)\right] \le P_{zz_{max}} \end{aligned} \tag{25}$$

Care must be taken in the application of Eq. (25) as a constraint, as the denominator is small. This makes taking the gradients of the constraint problematic for the numerical solution algorithm and can lead to instability. However, it can be shown as in [43], that the denominator is always positive. A singular denominator would mean an infinite uncertainty at that point, a condition which is not possible after the initialization. Therefore, with a positive denominator, the constraints may be rewritten in γ to avoid any numeric instability as:

$$\begin{aligned} \zeta_2(t_f) - P_{xx_{max}}\left[\zeta_1(t_f)\zeta_2(t_f) - \zeta_3^2(t_f)\right] &\le 0 \\ \zeta_1(t_f) - P_{zz_{max}}\left[\zeta_1(t_f)\zeta_2(t_f) - \zeta_3^2(t_f)\right] &\le 0 \end{aligned} \tag{26}$$

4.3. Pseudospectral Methods

With the optimal control problem of Eqs. (15)-(18) defined, it is solved recursively, using an update of current position and target position estimates for each iteration. Efficient pseudospectral methods have made real-time solutions of the optimal control problem not only possible, but a topic of great interest [28, 30, 44-48]. The methods are treated extensively in [49-52] and are not re-derived here. For this research, GPOPS was employed using the Radau Pseudospectral Method as defined in [53]. An hp-adaptive algorithm, detailed in [54], was also used to check the accuracy of the approximation between nodes, breaking the problem into phases to handle discontinuities or increasing the degree of the polynomial approximation as required. Analytic partial derivatives of the cost function, constraints, and differential algebraic equations were used for speed and accuracy. The formulas are straightforward to compute, and are thus omitted.

4.4. The Unscented Kalman Filter

The core of the observability problem is in the relative coordinates between the observer and the target of interest. Bearing-only sensor measurements are linear in a polar coordinate system, as are limitations on maintaining the target within the camera FOV. Use of an exclusively polar system, however, requires transformation of the own-ship position estimates, ground avoidance constraints, and the naturally decoupled dynamics of the quadrotor system—all linear in the Cartesian frame. The nonlinear Cartesian-polar conversion problem is ubiquitous in tracking and navigation applications. The EKF is the most common approach to addressing it, but biased estimation and covariance matrix ill-conditioning are possible, causing premature collapse of error estimates and subsequent filter instability. This is particularly a problem when the degree of nonlinearity is high, or when the initial estimates for mean and covariance are significantly off [55].

For this research, an Unscented Kalman Filter (UKF) was selected for target position estimation after favorable performance comparison with an EKF. The UKF provides an unbiased error mean and covariance estimate to second order without the need to calculate derivatives [56]. This was implemented in the Cartesian formulation, using the Unscented Transformation (UT) for the measurement update vice the system propagation step, as early system testing showed a slight improvement in calculation time over the polar form.

Several variants of the UKF can be optimized for different applications, varying such factors as the selection of the sigma-points within the necessary conditions, choosing the regression weights, and performing the transformation to different orders of accuracy. For this research, propagation was performed with the linear transformation from Eq. (8), and the specific algorithm developed in [43] was used for the measurement update of the relative position states. During the actual flight test, the UKF and the trajectory planner were run serially, with measurements being received in parallel. As multiple measurements often became available during trajectory calculation, all new measurements

were processed in batch at each epoch.

5. IMPLEMENTATION

Applying an RTOC system to actual hardware presents challenges that may not exist in simulation. Requirements such as communication protocols, variable scaling, and sensor integration are typically very system specific, and omitted from this paper beyond the basic description. However, the framework required, and the challenges that stem from computational delays involved in solving the optimal control problem at each epoch are described in sufficient detail as they are germane to every RTOC system. To this end, the quadrotor testbed is first briefly reviewed, followed by the RTOC algorithm implementation strategy and some of the issues addressed.

5.1. Quadrotor Testbed Description

An in-house, custom-built quadrotor (Figure 3), designed at the Air Force Institute of Technology's (AFIT) Advanced Navigation Technology (ANT) Center, was selected and modified to demonstrate the efficacy of the control algorithm—particularly that of the real-time optimal control aspects—beyond simulation.

The aircraft consisted of a 60.7-cm square frame with four 22.86-cm blades driven by AXI Goldline 2212/20 brushless motors. Phoenix 25 speed controllers powered by two Li-Polymer 2200 mAh, 11.1 V, 3 cell batteries regulated the control signal. A simple 'U' shaped hook with an approximate 6 inch opening fabricated from welding rod was used to catch the power line, with dampening lines affixed to reduce hook vibration. A Pico-ITX (Ubuntu) with a VIA C7 1-GHz processor, 1-GB of RAM was used for data collection and image processing from a Logitech Quickcam Pro 9000 webcam.

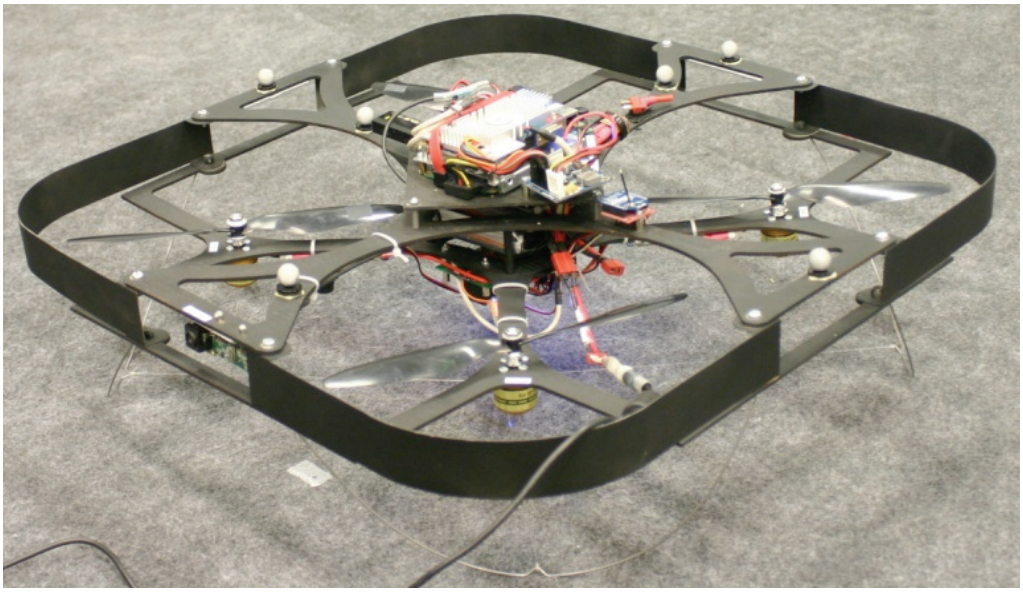

Figure 3. ANT Center Quadrotor

Accelerations were measured with an Analog Devices ADIS 16355AMLZ MEMS-IMU, and inner-loop flight control processing was performed on a custom PIC 24 microcontroller circuit board. Outer-loop RTOC guidance was provided by an algorithm running in Matlab® R2009a (Microsoft XP), and mid-loop control commands were generated using custom code written in C, using a GTK graphics processor packaged into a ground station hosted on Linux (Ubuntu). Both systems were running on Dell 360 2.0-GHz laptops with 2-GB of RAM, and signals were sent via a 2.4-GHz XBee Pro serial modem. Position feedback and flight test data were provided with a Vicon Tracker motion capture system using 60 nearIR (~750nm) cameras. A schematic of the overall system is shown in Figure 4.

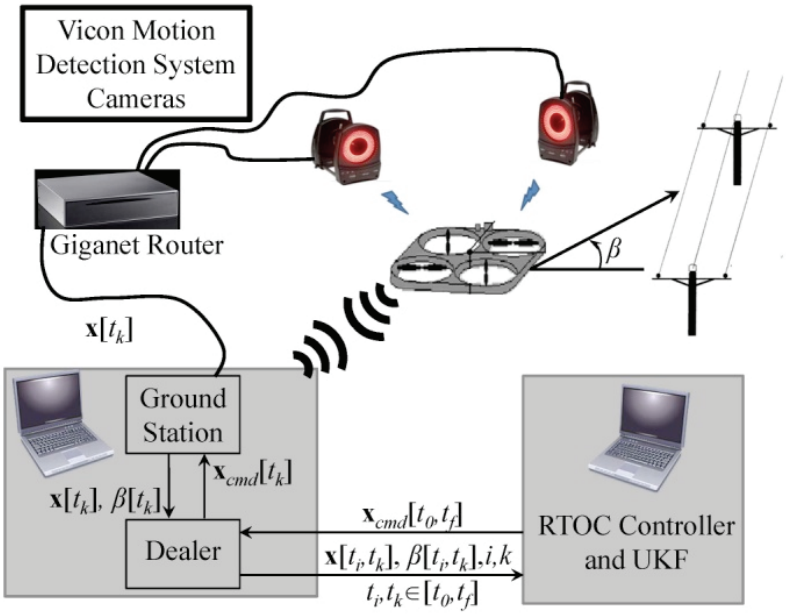

Figure 4. System Overview

A simplified flow diagram for the flight control system developed for this project is shown in Figure 5. The counter-rotating propeller pairs of the quadrotor allowed for control that was unusual, in that vertical, horizontal, and heading angle acceleration control could be essentially decoupled (a convenient simplification, though not required for the RTOC system in general). During each iteration of the RTOC algorithm, a complete optimal path was generated from the expected initial position to landing, and control during flight test was applied as tracking of that path, vice the more desirable feed-forward optimal control with feedback corrections. As a fully autonomous system, each optimal path sent to the controller concluded with a "missed-approach" game plan to execute if the appropriate certainty was not obtained in a defined time. Upon reaching the approach point with the required target position certainty, the flare segment is entered, altering the path to engage the hook and appending a new contingency option for what to do if the wire was not engaged as planned. For the flight test runs, bearing measurements from the webcam on the quadrotor were not available, so measurements from the Vicon system, corrupted with noise, were used as a representative substitute.

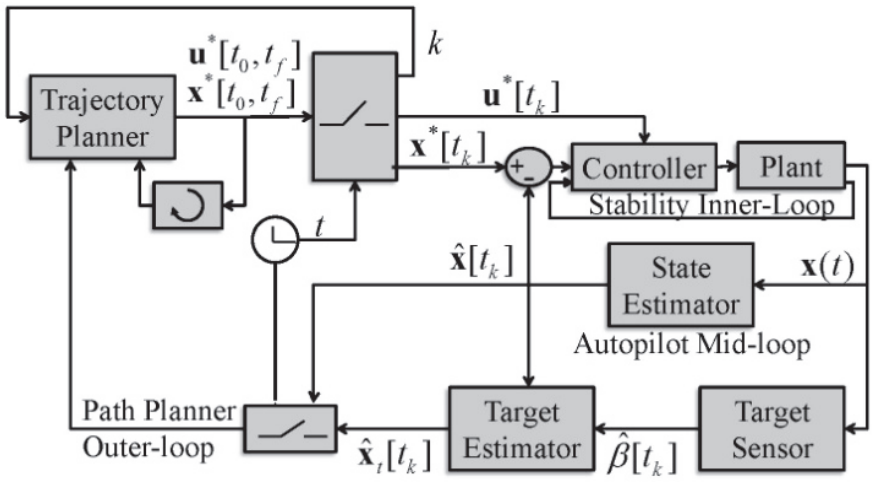

Figure 5. General Control Flow

5.2. RTOC Algorithm

The basic structure of the algorithm is iterative—as the recursive estimation filter provides better coordinates for the target, the trajectory planner provides updates to the optimal path, which will take the vehicle between provided boundary conditions $\mathbf{x}_0$ and $\hat{\mathbf{x}}_{app}$. The path that returns at each epoch is semi-discrete—containing all information required to reach the approach point, $\{\mathbf{x}_k^*(t),\mathbf{u}_k^*(t)\},t\in[t_k,t_f]$. For actual implementation, the functions are expressed as a discrete sequence with a fixed time step, splicing on any "pre-run" commands from initial takeoff to a "start test" hover position, and "post-run" commands for missed approach and the flare segment. A basic flow overview is shown in Figure 6.

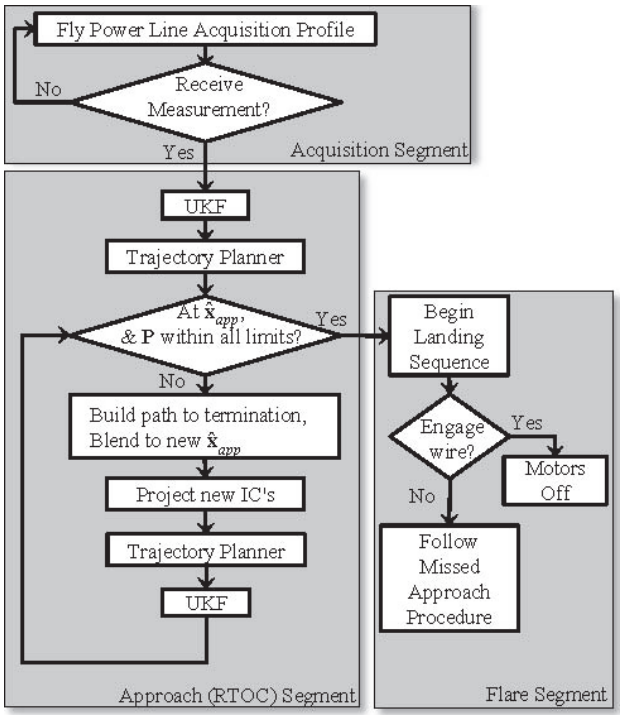

Figure 6. The RTOC Algorithm

The acquisition segment is completed when the power line is identified by the sensor, and an initial target estimate and trajectory are initiated. Since the initial target estimate and covariance are provided as a guess to the UKF based on likely height of the power line and likely sensor acquisition range, an initial trajectory can also be pre-calculated off-line, and used to seed the trajectory planner's initial guess. This is not required, since direct methods are tolerant of poor initial guesses, but it speeds the initial move. After the first pass of the trajectory solver, the previous epoch's solution is always used for the initial guess, trimming off the initial portion that should have already been flown. Once the main approach segment loop is entered, it is executed until the vehicle reaches the approach point with the required certainty in the target location.

Counter intuitively, note that the main loop call to the UKF happens *after* the trajectory planner. The trajectory planner consumes most of the loop time, Δt_{calc}. Other steps are fast, and with a slow sensor update rate, it is not likely that new measurements will arrive between the time the UKF provides an estimate and the time the trajectory planner begins calculations on the next epoch. During those calculations, however, multiple measurements will likely have been received, and the target estimate (and thus the approach point estimate) should incorporate the new measurement data prior to checking to see if the approach point has truly been achieved and the required certainty has been met.

5.3. Special Initial Condition Considerations

Two special considerations are addressed with respect to the setting of initial conditions for each epoch of the path planner. If the optimal control was applied to the vehicle, but the actual position varies

significantly from the expected optimal trajectory, some modeling error or disturbance is present, most likely wind for this application. The tracking error should be integrated, and the model should be updated with a wind estimate entered in the next epoch's problem formulation, as detailed in [57]. For the flight test in the still air of the indoor flight facility, wind disturbances were found to be very minor, other than from turbulence near the wall during the actual hooking process. This however was during the flare segment, when the optimal control algorithm is no longer running. The normal error integration of the flight control system was found to be sufficient to handle all disturbances.

A more significant implementation problem occurs when the initial conditions are outside of the allowable flight envelope. Recall that the FOV lines and safe approach line are defined relative to the current target estimate, and therefore the boundaries move with each target position update of the UKF. If the vehicle is on or near one of these boundaries at time t_k and the UKF for epoch t_{k+1} moves the target closer horizontally to the vehicle, the initial conditions for epoch t_{k+1} can be outside of limits, resulting in no possibility of a feasible solution from the trajectory planner. All initial conditions must be checked for validity, and moved into a valid flight envelope if necessary. If required, a smoothing function can be applied as will be discussed in Section 5.4.

5.4. Variable Calculation Time

For simplicity of process integration, researchers working in RTOC typically choose to update the optimal solution at a fixed loop time, Δt_{calc}. This allows the flight control algorithm to look for a new optimal solution at a set time in the flight control calculation loop. The downside to this approach is that the trajectory planner must be finished prior to that time, mandating a very conservative Δt_{calc}, and sacrificing efficiency, as *every* iteration by definition, takes the maximum allowable iteration time. Allowing a variable loop time has the advantage that the flight control algorithm can use the optimal solution as soon as it is available in each loop, or can wait as long as needed until the optimal solution is found. The downsides are coding complexity for timing transitions, and the fact that the projected initial conditions may not match the current commanded conditions at the new epoch.

A variable calculation time was used for this research, and Δt_{calc} was set as the *expected* calculation time, vice a maximum. The efforts of the flight control autopilot and the optimization software were processed independently, but threaded together to allow the optimal solution to be applied as soon as it was available. As an engineering safety valve, maximum iteration limits were still set for the optimization software, but were not triggered during testing. The concept was that if the optimal solver was unable to converge on a particular instantiation of the optimal problem, it would be reset with the current conditions and target estimate, without using the previous solution as its initial guess. The system will continue to fly the last complete optimal trajectory until a new one is provided.

When the trajectory planner provides an optimal solution earlier than expected, the effects of variable calculation timing are transparent. The new portion of the optimal solution is simply appended at the time the solution was expected to be available, and the previous epoch's path is flown until that point, guaranteeing a continuous solution. For solutions that are available later than expected, however, a discontinuity is possible in the state and control. This can be seen in Figure 7 at time t_{k+1}. The error between the actual state and the planned state as each old solution is replaced is now a factor not only of how close the vehicle tracks the planned state, but also depends on the distance and direction the vehicle has traveled in the amount of time the calculation took beyond that which was expected. Another discontinuity occurs at the approach point, at the end of the path. While the trajectory planner is calculating, new measurements are still being received, and the estimate of the target location will now be at $\hat{\mathbf{x}}^{+}_{t_{k+1}}$, though the path was planned to $\hat{\mathbf{x}}^{-}_{t_{k+1}}$. The cumulative effect is that by the time an optimal solution becomes available, it travels from a place the vehicle is no longer at, to a place it 'thinks' the target is no longer at. Some sort of blending strategy is required to ensure smooth, continuous control and to correct to the path ends.

There are optimal methods for resolving the differences in initial and final conditions, most notably those of neighboring optimal control (NOC) [27, 58]. For systems where these differences are critical, NOC is recommended. Experimentation with this system, however, suggested that the differences in initial conditions were very small, as the calculation timing was predictable, and the longest calculation observed was only 0.11 seconds beyond what was anticipated. Changes in the "tail" of the path can be more significant, occurring when the target estimate is moved while the optimal path is being calculated. Being at the end of the flight, however, an updated solution should be available before reaching the final portion until the end-game of the flight, when the target position is established and

changes are small. Blending was still used for both ends of the path, but the computational expense of NOC was forgone for a simple and efficient method that ensures a continuous command to the latest estimate of the target location.

To avoid generating sharp changes of trajectory with a linear blending method, a cosine wave was used to "round the corners" and smoothly transition the head or tail of the path to the corrected point. The details of the method can be found in [43]. Sample results of the cosine blending corrections can be seen in Figure 7, where the dark black line indicates the path that is sent to the vehicle at the actual update time t_{k+1}. This is a composite of the solid optimal solution at $\mathbf{x}^*_k$, the dashed solution at $\mathbf{x}^*_{k+1}$, and the dotted blending correction as a result of updating the target to $\hat{\mathbf{x}}^+_{t_{k+1}}$ during calculation time.

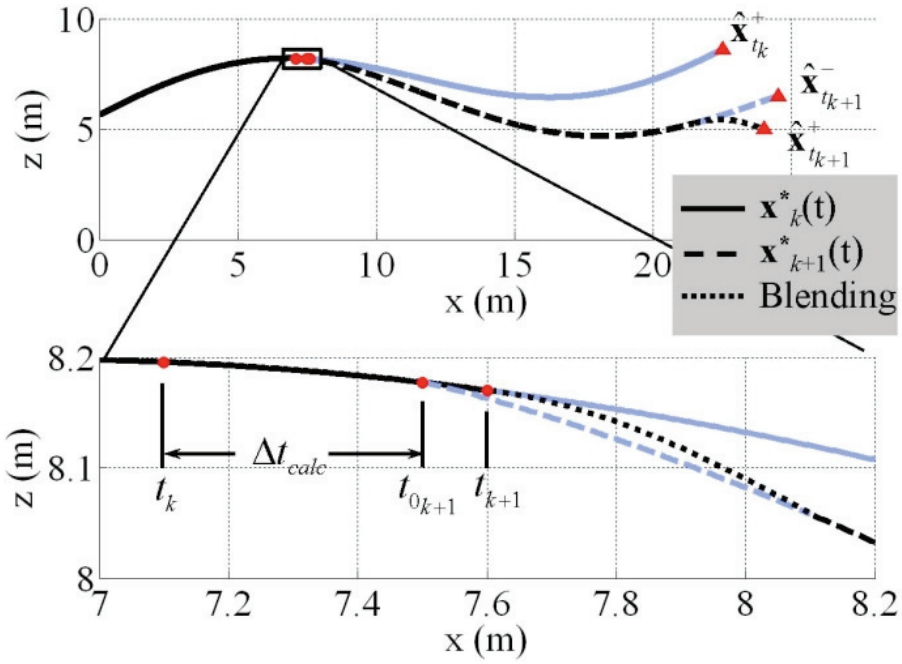

Figure 7. Cosine Blending Corrections

5.5. Process Threading

A final noteworthy implementation lesson came from timing synchronization problems stemming from using a flexible calculation time for the optimal trajectory planner on actual hardware. The UKF, trajectory planner, communication paths, autopilot processes, and speed control servos are each running iterative computation loops, but with asynchronous rates.

Threading loops with known rates is not difficult, but the trajectory planner has a variable cycle time (just over 1 Hz for this application). Working at a much faster rate (50 Hz), the autopilot must have a buffer of future commands to process. To achieve this, a "dealer" function was implemented, running between the processors for the trajectory planner and the autopilot—see Figure 4. The dealer checks for an updated path (the "deck" if you will), and provides the current vector of commands during each cycle of the autopilot. The slower trajectory planner sends the updated path whenever it is complete via TCP packets with a blocking protocol to stop computation until the path is picked up by the higher rate dealer (100 Hz). This keeps communication delay on the order of the dealer function computation loop. A similar method was used in the other direction to get measurements, limits, and initial conditions into the RTOC process, stopping the slower processor after sending a "ready" poll, checked for during each loop of the dealer. With this technique, slowing down the trajectory planning loop to allow a fixed calculation time is not necessary.

6. RESULTS

The RTOC system was validated through extensive simulation during development, and flight tested to verify the algorithm and its capability to accomplish the mission. The full-scale flight test profiles were performed in the AFRL/RQ μAVIARI Indoor Flight Test Lab. An average medium voltage (distribution) utility pole is approximately 10 m high, but the safe maximum height for tracking camera reception in the indoor flight facility was 5.5 m. The walls of the facility dictated a maximum usable range of approximately 18 m, well inside of the expected range at which a power line could be confidently identified with a webcam type sensor. Correspondingly, the flight test was scaled down in size to fit the μAVIARI, and speed was reduced to match a likely approach segment time of about 30 seconds.

6.1. Simulation Results

In order to verify the robustness and reliability of the estimation and optimization algorithms, a Monte Carlo-style simulation of 1,000 runs was performed on the same scale as the flight tests to maintain comparability. The run number was pre-selected, and the resulting solution parameters of average loop time, mean error, and final directional covariance converged to within 10^{-3} of their respective units. The problem geometry was varied by moving the actual target location from the initial estimate, $x_t \sim \mathrm{N}\ (\hat{x}_{t_0}, 49\mathrm{m}^2)$, $z_t \sim \mathrm{N}\ (\hat{z}_{t_0}, 4\mathrm{m}^2)$ limiting outliers to staying within the allowable flight space vertically, and limiting the initial pickup range to at least 12 m to provide some minimal maneuver room to use the system (the longest run was 38 m). Real-world considerations must include a contingency plan for a "go-around" for exceptionally late or missed sensor pickups. The difference in vertical and horizontal certainty reflects the fact that more knowledge will exist concerning the height of the power line than of the initial sensor pickup range. For a full-scale system, actual sensor capability, an estimate of power line height variance, and the amount of confidence in the mapped power line locations should be included in the selection of $\mathbf{P}_0$. Disturbances from effects such as wind gusts were added with a bivariate Gaussian distribution, adding a random variance in the vehicle location, $\mathbf{x}_{err} \sim \mathrm{N}\ (0.0.25\mathrm{m})$, measured by the own-ship navigation system. The simulation was initiated with the conditions found in Table 1.

Table 1. Simulation Parameters

Parameter	Value	Parameter	Value
Est. Loop Time	0.9 s	$P_{xx_{max}}, P_{zz_{max}}$	0.02 m^2
β_{min}, β_{max}	-30°, 40°	App. Offset (m)	$[-2 \quad 0.4]^{\mathrm{T}}$
σ_β	4°	$\hat{\mathbf{x}}_t$ (m)	$[9 \quad 4]^{\mathrm{T}}$
$\lvert v_x\rvert_{max}, \lvert v_z\rvert_{max}$	0.5 m/s	$\tilde{\mathbf{x}}_0$	$\left[-8 \quad 3 \quad 0 \quad 0 \quad P_{xx_0}^{-1} \quad P_{zz_0}^{-1} \quad 0\right]^{\mathrm{T}}$
$\lvert u_x\rvert_{max}, \lvert u_z\rvert_{max}$	0.5 $\mathrm{m/s}^2$	$\mathbf{P}_0$ (m^2)	$\begin{bmatrix} 80 & 0 \\ 0 & 80 \end{bmatrix}$
z_{min}, z_{max}	0.8, 6 m		

The shape of each instantaneous optimal trajectory varies based on the information available to the system at the time. Figure 8 shows typical solutions, with specific problem parameters varied to highlight key features. The results show complete trajectories for the remainder of the flight, as are provided at every epoch by the trajectory planner. The characteristics shown are helpful in creation of heuristics to mimic the optimal solution, potentially a requirement for small UAVs without processing capacity for RTOC. All maneuvering in the simulation is restricted to the vertical plane. Generally, the horizontal length of the run (note the asymmetric axes lengths) allows a greater amount of information to be collected about the vertical position of the target, requiring the trajectory planner to move away from the initial LOS angle for range information.

Figure 8a shows the characteristic shape for the typical initial conditions, where the system is directed to climb to the maximum allowable altitude, or ceiling, for a "high look," moving to obtain a "low look" at the end game where the measurements are more effective due to the close range. This path visually increases the information elements seen in Eq. (12). FOV limitations keep the vehicle in

a position where the target will be visible to the fixed camera, and a "safe approach" line is enforced to keep the aircraft from flying past the desired approach point and backing up. Though certainly within the capabilities of the quadrotor, it was deemed unsafe to intentionally proceed inside the approach point until the certainty in the actual power line position was within the required limits.

The second panel, Figure 8b, shows an instantaneous flight trajectory with the allowable flight envelope limitations removed, maintaining the speed and acceleration limits in the dynamic constraints. The final required target position certainty was increased to highlight the fact that the optimal solution may intentionally include transients inside of the safe approach line if not enforced.

The third panel, Figure 8c, shows the path solution for a camera with a more restrictive total FOV (30°). The most extreme target approach angle is held as long as necessary. For times when the final certainty requirements do not differ greatly from the current covariance estimate, only a small excursion is necessary to gain the needed amount of information, as shown in Figure 8d.

Obviously, every active parameter in the optimal control problem contributes to the final shape of the trajectory, but the sensitivity of a few dominant parameters found during the research was considered noteworthy. The immediate move away from the initial LOS angle is predictable. The "hook" at the end of the path shown in Figure 8ac is also dominant, taking advantage of the wide angular spectrum at close range for the greatest increase in information. For a workable heuristic, the initial move away from the first LOS angle provides the range observability necessary to determine when to make the "hook," which could be initiated at the 6 m remaining point at this speed. Though the characteristic shape is the same, the range at which the "hook point" is executed is nonlinear and not directly scalable to a larger/faster problem. To find it for a particular system, the algorithm should be run with system specific limitations.

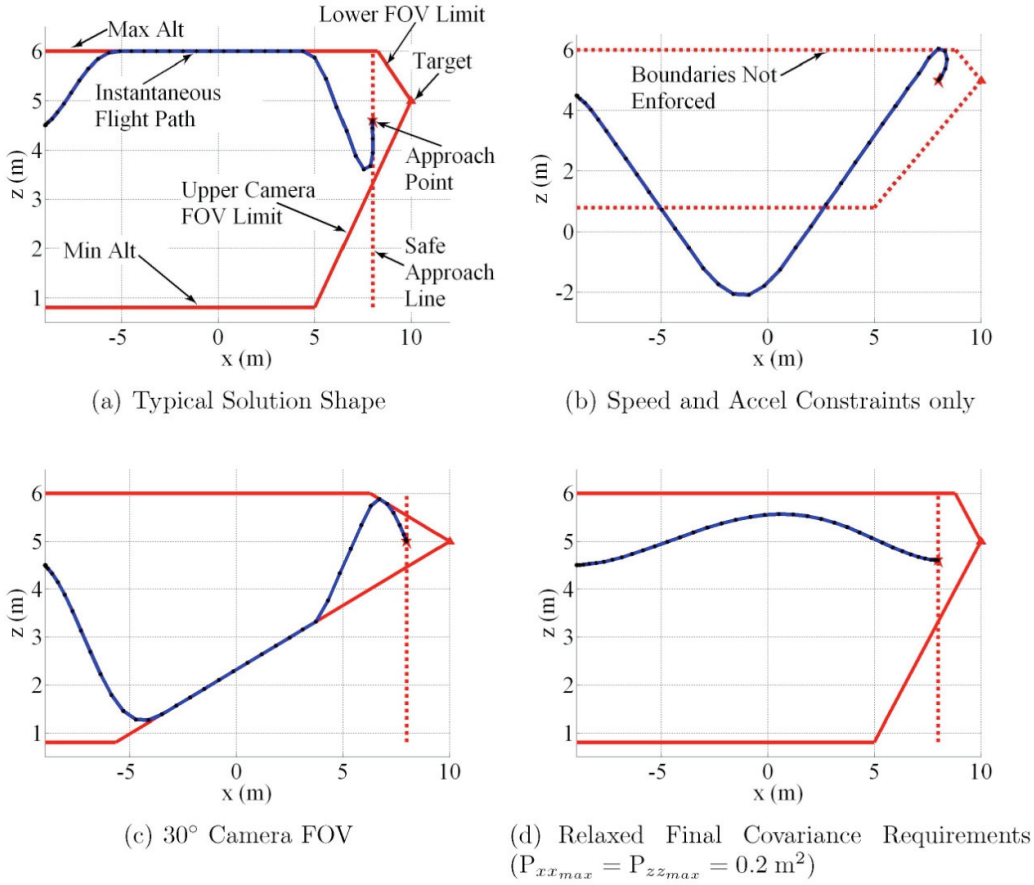

(a) Typical Solution Shape

(b) Speed and Accel Constraints only

(c) 30° Camera FOV

(d) Relaxed Final Covariance Requirements ($P_{xx_{max}} = P_{zz_{max}} = 0.2\ m^2$)

Figure 8. Instantaneous Trajectory Shape Sensitivity to Constraints

6.2. Local Minima

The geometry of the problem creates a bimodal solution space. With symmetric constraints and no initial velocity, a path with an initial move up would have a mirrored path with an initial move down and the same total cost. Global favorability of a "high road" versus a "low road" local minimum is dependent on the initial state and constraints when the first measurement becomes available. For heuristics, the overall direction tends to be high if the initial position of the vehicle is low relative to the target, and vice versa. Stronger factors are initial velocity (tends to continue in the initial direction) and the vertical difference between the approach point and the actual height of the target. Due to the minimum time weighting and the "hook" at the end switching from one extreme to the other, if the approach point is lower than the target, the path with start high and end low and vice versa –note the final approach point difference between Figure 8c and Figure 8d. The amount of maneuvering room between the altitude limits and the current target position estimate also impacts this decision.

As the optimal solver can guarantee only local minima, knowledge of the likely shape of the global solution can be used to bias the initial guess to the desired channel (by choosing a high or low mid-point in addition to the end points typically supplied). Furthermore, the first path can be solved for based on the initial relative target location guess, before the first measurement is received. Since the vehicle will actually start following this path while the solver is producing the first post-measurement path, the initial conditions for the first post-measurement path will already have been biased, "committing" the vehicle in the desired direction.

For the second run of the full-scale flight test, the initial target estimate was intentionally placed unrealistically near the ceiling limit, making the "low road" the initial global minimum and forcing motion in that direction. Once the vehicle commits to a vertical direction, changing to the other extreme becomes costly in terms of additional control and extra time near the "middle" of the flight envelope where there is little observability in range. Though unlikely, the "low road" scenario was demonstrated because it could possibly be encountered with a bad enough set of measurements. In the lab, the initial relative position of the power line was fixed, and the initial target position estimate was varied to cause the difference in path selection. In a true UAV landing scenario, the initial relative target estimate will be fixed for every run (based on the likely parameters of the UAV at initial sensor pickup). The initial solution will therefore be the same for every run, and the vehicle will make the first move in the direction known to be the global minimum during the first calculation epoch.

6.3. Timing and Accuracy

For the 1,000 simulation runs, the average loop time, including optimization calculation, communication, UKF calculations, and all delays was 0.82 s, with a standard deviation of 0.022 s. Figure 9 shows the advantage of using variable calculation timing. If a fixed timing update was selected based on this data, it would be about Δt_{calc}=1.3 s, and no trajectory updates would have been available until that time for each epoch. Additional complexity in the creation of the dealer function was required to be able to accept updates as soon as they were available, but 59% more path updates were received, greatly increasing the system's flexibility and ability to deal with uncertainty.

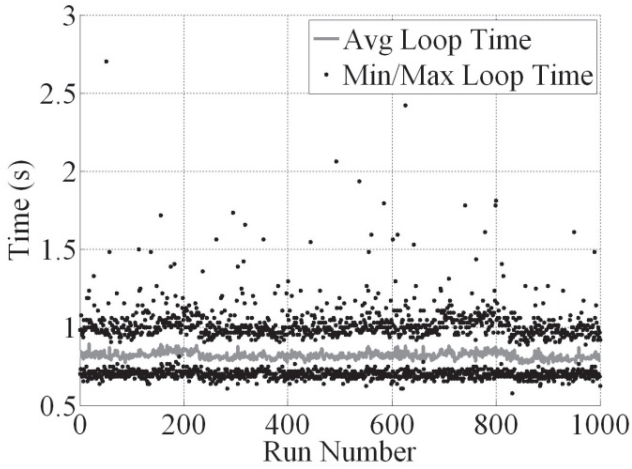

Figure 9. Average Loop Times for Simulation Runs

The system's final error upon reaching the approach point is shown in Figure 10. As expected, the certainty of the vertical component is better than required, due to the number of highly orthogonal measurements for the entire flight (variance of the series of final vertical error estimates from the 1,000 simulation runs was 0.0026 m^2).

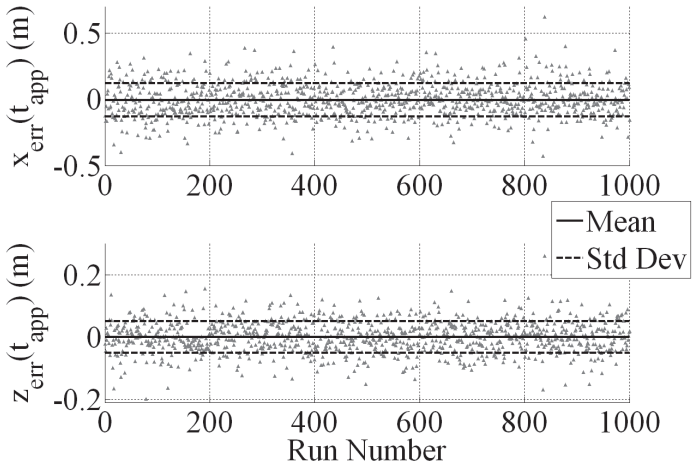

Figure 10. Final Target Estimate Error for 1,000 Simulation Runs

The average of the final horizontal covariance estimates was 0.017 m^2, which closely matched the actual variance of the final horizontal error of 0.016 m^2. The estimated covariance requirement was to be below the limit of 0.02 m^2, but was slightly better than expected due to the fact that typically 2-3 measurements come in during each planning cycle. If the first measurement is the one that put the variance under the limit, the effect of all three is still recorded, as they are processed in batch. For error planning with the poor measurement quality allowed, the worst-case quadrotor command will be within 0.305 m (one foot) of the actual approach point 97% of the time. Even at that extreme, when including the additional close-range measurements obtained after the approach point on the way to the wire during the flare, the accuracy of the estimate at the time of landing was well within the size of the hook, even accounting for the error of the quadrotor's true position. These numbers can be adjusted to any particular desired level—the important result is the validation of the algorithm's effectiveness at accomplishing the primary purpose of the research—to create a path in real-time that can achieve a particular amount of target position certainty in a stochastic environment while executing a primary mission task.

The time series results of the simulation runs can be seen in Figure 11 and Figure 12. The extended times for some runs were due to a more distant simulated target location. These results show the stability and predictability of the UFK algorithm, and the ability to achieve the final required covariance estimate.

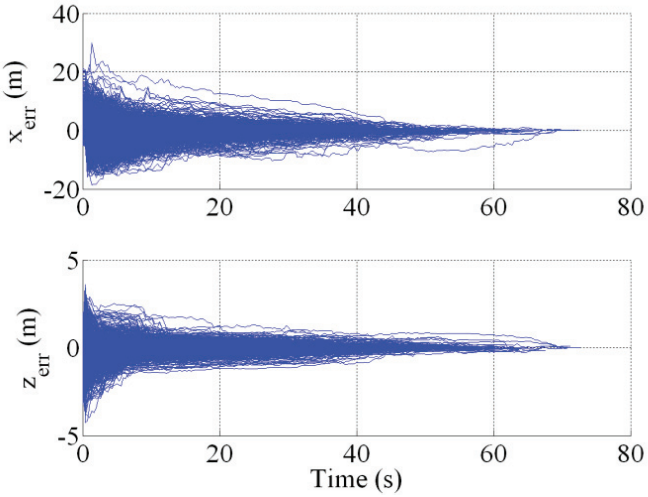

Figure 11. Target Position Estimation Error During 1,000 Simulation Runs

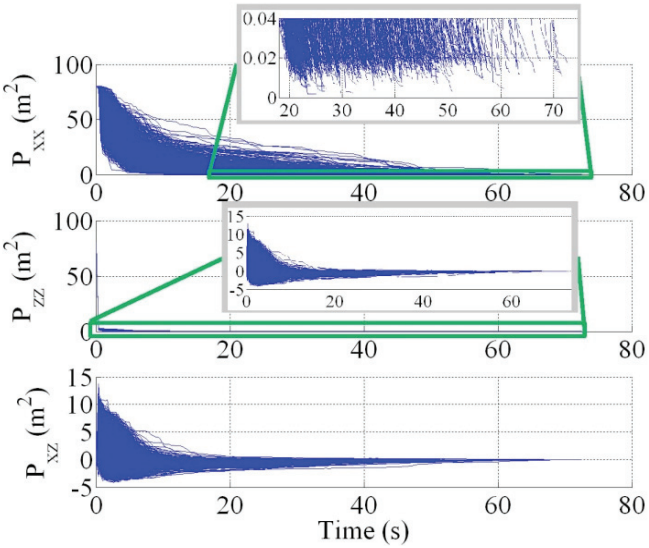

Figure 12. Target Covariance During 1,000 Simulation Runs

6.4. Flight Test Results

Flight test for the system included a build-up approach series of flights initially working with the stability of the system, followed by the path tracking capability in a small flight facility at the AFIT ANT Center. The dealer program was incorporated to command simple flight profiles, eventually adding the path planning system. Further flights were accomplished to test flying qualities with the arresting hook, adding damping lines to reduce unwanted vibration modes. Scaled down profiles were used to test the flare segment control and land on an actual wire.

Full-scale profile flights were first accomplished with a simulated wire in the larger AFRL µAVIARI, followed by the final two end-to-end tests conducted with a real wire to demonstrate the complete system from takeoff to perching on the power line. The only human input to the system for the full-profile flights was consent to turn the motors on and off. The two end-to-end tests were initialized in the same manner as the simulations, with the exceptions noted in Table 2.

Table 2 Flight Test Parameters and Results

Parameters	Run 1	Run 2
$\mathbf{x}_0$ (m)	$[-8 \quad 3]^T$	$[-8 \quad 3]^T$
$\mathbf{x}_t$ (m)	$[8.54 \quad 4.17]^T$	$[8.54 \quad 4.17]^T$
$\hat{\mathbf{x}}_{t_0}$ (m)	$[\ 4 \quad 3\ ]^T$	$[\ 15 \quad 5\ ]^T$
Results		
Avg Loop Time	0.83 s	0.85 s
Min Loop Time	0.77 s	0.77 s
Max Loop Time	0.92 s	0.97 s
RTOC Segment	31.53 s	32.33 s
$\mathbf{x}_{error}(t_{perch})$ (m)	$[0.0117 \quad 0.0144]^T$	$[0.0247 \quad 0.0298]^T$
$\mathbf{P}(t_{app})$ (m^2)	$\begin{bmatrix} 0.0195 & 0.0025 \\ 0.0025 & 0.0024 \end{bmatrix}$	$\begin{bmatrix} 0.0185 & -0.0024 \\ -0.0024 & 0.0024 \end{bmatrix}$

Figure 13 shows a progression of solutions in the vertical plane for the full-scale Run #1 at separate sample times. The arrows from the vehicle denote the actual noise-corrupted bearing measurements received by the system in batch (delayed), and both the estimated and actual target location can be seen. For visualization, the covariance ellipsoid shows a 95% likely confidence ring, and the error in the initial seconds exceeds this slightly. The range ambiguity can be seen in the orientation of the ellipse. The reason for the "hook" at the end of the path is clear, as the path planner moves the vehicle to a position orthogonal to the greatest axis of remaining uncertainty. The diamonds denote target estimate histories.

Figure 13d shows the comparison of the actual path that was flown by the vehicle with the path that would have been commanded had the target position estimate always been perfectly accurate. This demonstrates the true power of stochastic real-time optimal control. Even with the initial error in the

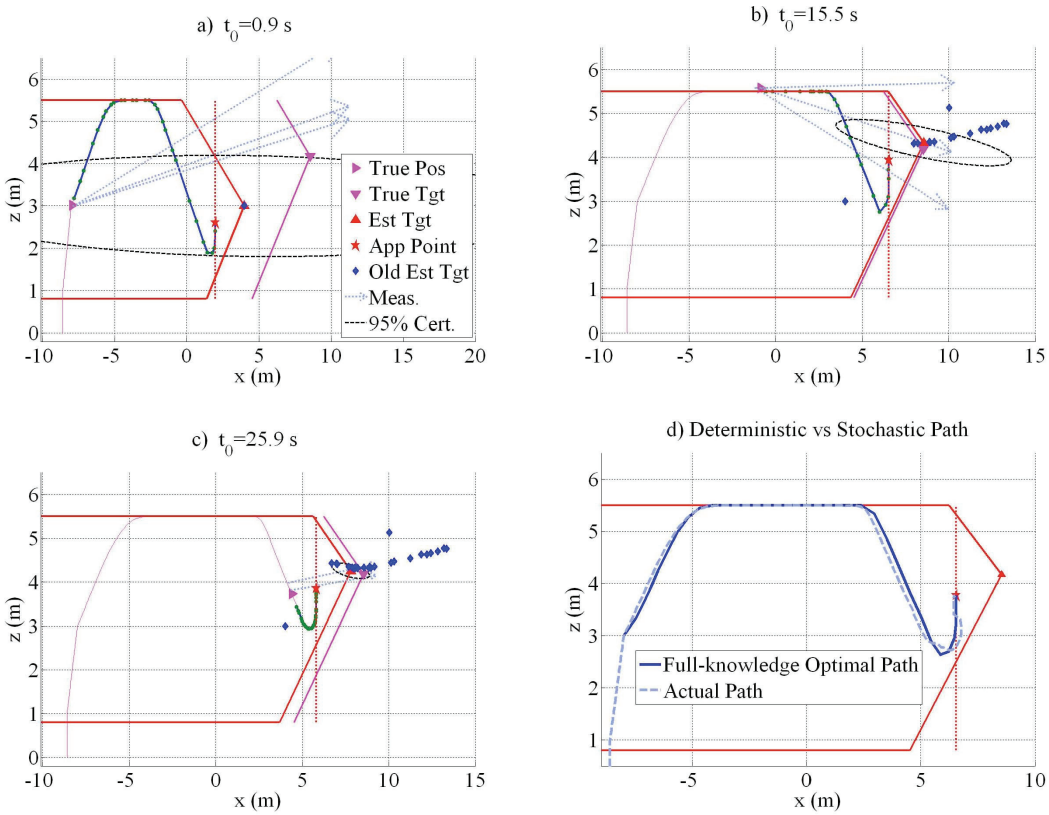

Figure 13. Flight Test Run #1 Snapshots, and Comparison to Full-Knowledge Optimal Path

target position, and with the errors in each measurement, the actual path that the vehicle flew was very close to the perfect-information solution.

As previously mentioned, the initial target estimate for the second test flight profile was set unrealistically high, making the "low road" the global minimum due to the insufficient observability of the horizontal axis while near the maximum allowable altitude. A snapshot progression is shown in Figure 14. Once a direction has been committed to, the initial conditions of each epoch make the "low road" the global minimum for the duration, even with the resolving true target location. In terms of mission accomplishment, the only loss from the perfect-information solution in this contingency case was a small increase in flight time, 0.8 s.

Figure 14d, is a snapshot of the flare mode. For the quadrotor, the path simply moves directly underneath the wire, slowing as it approaches from Eq. (32), and descending to engage the hook, as shown in Figure 15.

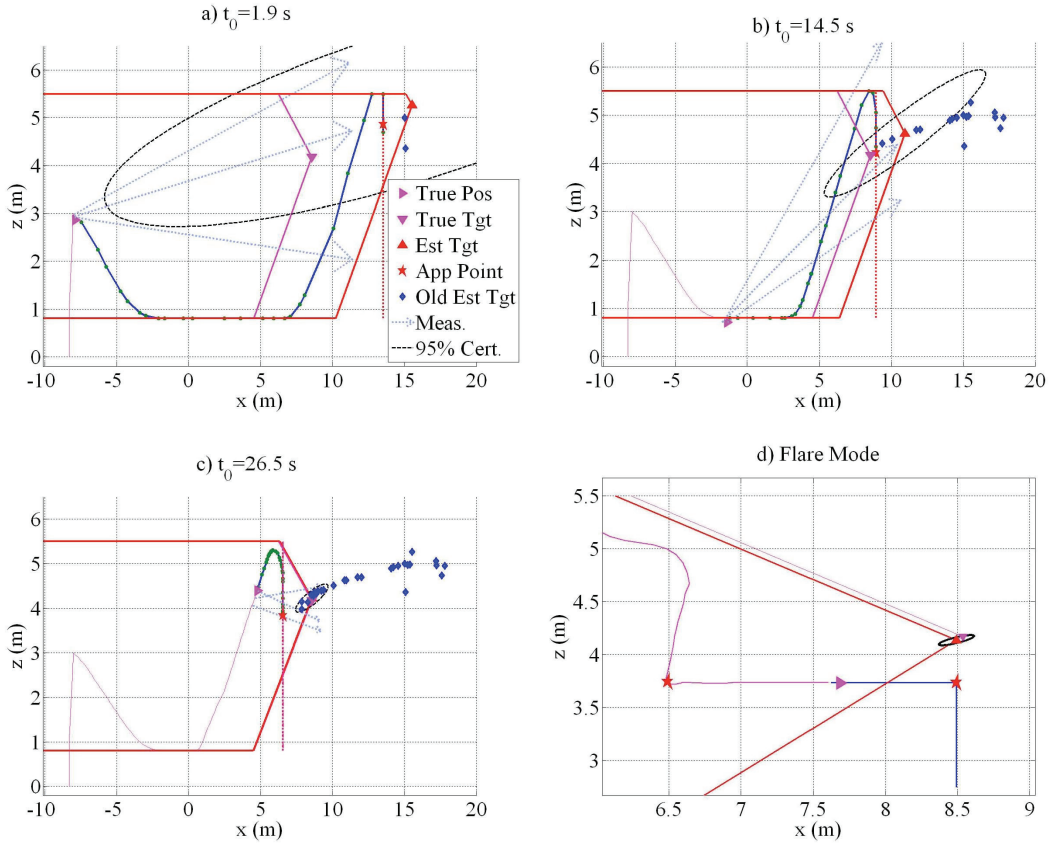

Figure 14. Snapshot Progression of Flight Test Run #2

7. CONCLUSIONS

This research successfully developed a method to simultaneously solve the optimal control and the optimal estimation problems. A recursive algorithm was designed to implement the method in real-time for disturbance rejection and treatment of uncertainties in the model and measurements. The solution is comprehensive, and was verified in flight test—autonomously landing a quadrotor on a wire as an enabler for the future capability of energy harvesting. Implementation techniques for variable solution timing were provided and shown to be effective, and blending methods were included to address potential discontinuities.

The optimal control formulation presented offers a solution which does not require the prescription of a final time (or equivalent), producing a much greater level of flexibility for potential optimal solutions. Inclusion of information requirements in the constraints allows use of a vehicle-specific cost function, and provides a solution that does not waste effort in information collection beyond that which

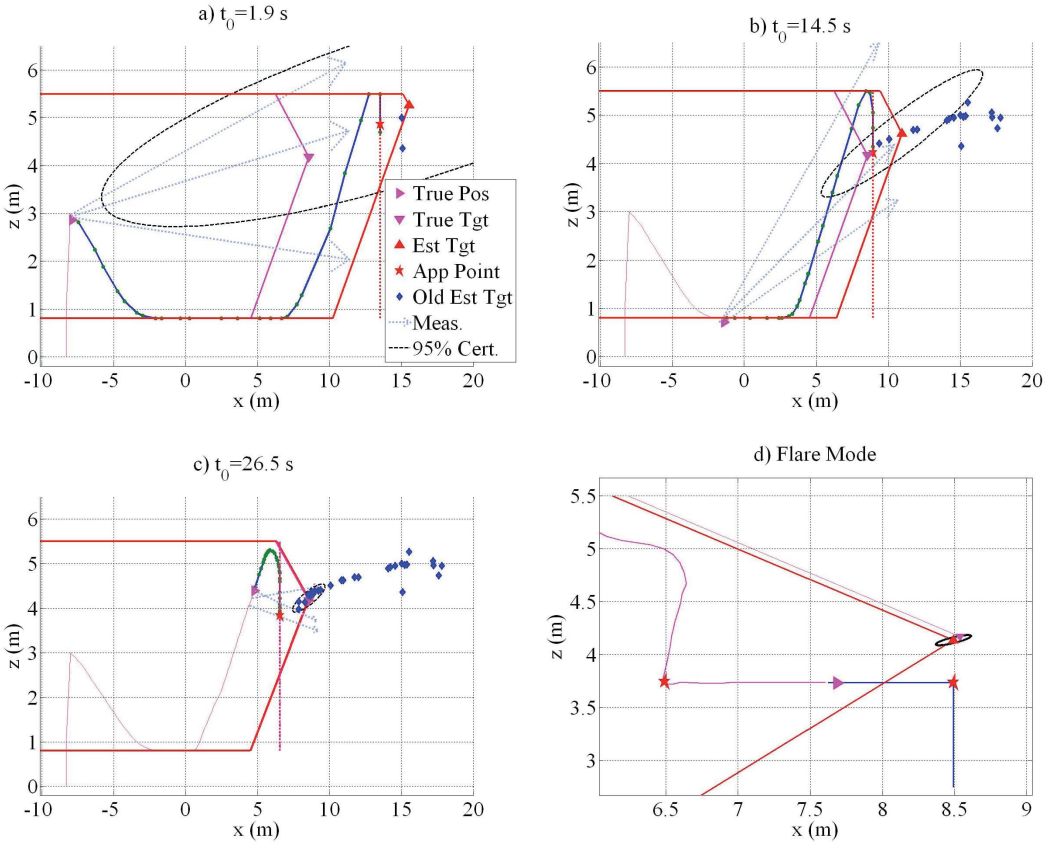

Figure 15. Quadrotor Just Prior to Hook Engagement

is required for mission accomplishment. In addition, because it is not necessary to compress the information metric into a scalar, directional information is retained, and the shape of the desired certainty ellipsoid can be defined based on the equipment requirements. The principles of the method may be applied to any system with a bearing-only sensor that requires relative position information about a source in order to perform its primary mission.

ACKNOWLEDGMENTS

The authors gratefully acknowledge the support of the Air Force Research Laboratory, AFRL/RQ, with funding and the use of the indoor flight test facility, and also acknowledge the coding assistance of Mark A. Smearcheck in the development of the communication structure and the implementation of the flight control system onto the quadrotor.

REFERENCES

[1] Lindgren, Allen G. and Kai F. Gong. “Position and Velocity Estimation via Bearing Observations”. IEEE Transactions on Aerospace and Electronic Systems, AES-14(4):564-577, 1978.

[2] Liu, P.T., “An Optimum Approach in Target Tracking with Bearing Measurements,” *Journal of Optimization Theory and Applications,* Vol. 56, No. 2, 1988, pp. 205-214.

[3] Logothetis, A., Isaksson, A., and Evans, R.J., “An Information Theoretic Approach to Observer Path Design for Bearings-Only Tracking,” *Proceedings of the 36th IEEE Conference on Decision and Control,* Vol. 4, 1997, pp. 3132-3137.

[4] Nardone, S.C., and Aidala, V.J., “Observability Criteria for Bearings-Only Target Motion Analysis,” *IEEE Transactions on Aerospace and Electronic Systems,* Vol. AES-17, No. 2, March 1981, pp. 162-166.

[5] Oshman, Y., and Davidson, P., "Optimization of Observer Trajectories for Bearings-Only Target Localization," *IEEE Transactions on Aerospace and Electronic Systems,* Vol. 35, No. 3, July 1999, pp. 892-902.

[6] Passerieux, J.M., and Van Cappel, D., "Optimal Observer Maneuver for Bearings-Only Tracking," *IEEE Transactions on Aerospace and Electronic Systems,* Vol. 34, No. 3, 1998, pp. 777-7888.

[7] Ross, I.M., "Pseudospectral Feedback Control: Foundations, Examples and Experimental Results," *AIAA Guidance, Navigation, and Control Conference,* Vol. 4, 2006.

[8] Gong, Qi, Wei Kang, S. Bedrossian, Nazareth, Fariba Fahroo, Pooya Sekhavat, and Kevin Bollino. "Pseudospectral Optimal Control for Military and Industrial Applications". Proceedings of the 47th IEEE Conference on Decision and Control, 4128-4142. New Orleans, LA, December 12-14 2007.

[9] Benson, D., "A Gauss Pseudospectral Transcription for Optimal Control," Ph.D. Dissertation, Massachusetts Institute of Technology, 2005.

[10] Spiess, F.N., "Complete Solution of the Bearings Only Approach Problem," *UC San Diego: Scripps Institution of Oceanography, MPL Technical Memorandum,* 1953.

[11] Van Trees, H.L., "Detection, Estimation, and Modulation Theory, Part I." Wiley, New York, 1968.

[12] Maybeck, P.S., "Stochastic Models, Estimation, and Control," Vol. 2, Academic Press, New York, NY, 1982.

[13] Hammel, S., and Aidala, V.J., "Observability Requirements for Three-Dimensional Tracking via Angle Measurements," *IEEE Transactions on Aerospace and Electronic Systems,* Vol. AES-21, 1985, pp. 200-207.

[14] Hammel, S.E., Liu, P.T., and Hilliard, E.J., "Optimal Observer Motion for Localization with Bearing Measurements," *Computers and Mathematics with Applications,* Vol. 18, No. 1-3, 1989, pp. 171-186.

[15] Le Cadre, J.P., and Tremois, O., "Bearings-Only Tracking for Maneuvering Sources," *IEEE Transactions on Aerospace and Electronic Systems,* Vol. 34, No. 1, 1998, pp. 179-193.

[16] Le Cadre, J.P., "Optimization of the Observer Motion for Bearings-Only Target Motion Analysis," *Proceedings of the 36th Conference on Decision and Control,* Vol. 4, 1997, pp. 3126-3131.

[17] Helferty, J.P., Mudgett, D.R., and Dzielski, J.E., "Trajectory Optimization for Minimum Range Error in Bearings-Only Source Localization," *Proceedings of the Conference on Oceans '93,* Vol. 2, 1993, pp. 229-234.

[18] Helferty, J.P., and Mudgett, D.R., "Optimal Observer Trajectories for Bearings-only Tracking by Minimizing the Trace of the Cramer-Rao Lower Bound," *Proceedings of the IEEE 32nd Conference on Decision and Control,* 1993.

[19] Leung, C., Huang, S., and Dissanayake, G., "Trajectory Planning for Multilple Robots in Bearing-Only Target Localisation," *IEEE/RSJ International Conference on Intelligent Robots and Systems,* 2005, pp. 2312-2317.

[20] Ponda, S.S., Kolacinski, R.M., and Frazzoli, E., "Trajectory Optimization for Target Localization Using Small Unmanned Aerial Vehicles," *AIAA Guidance, Navigation, and Control Conference,* 2009.

[21] Skoglar, P., Orguner, U., and Gustafsson, F., "On Information Measures based on Particle Mixture for Optimal Bearings-only Tracking," *IEEE Aerospace Conference Proceedings,* 2009, pp. 1-13.

[22] Feldbaum, A.A., "Dual Control Theory I-IV," *Automation and Remote Control,* Vol. 21, 22, 1960-61, pp. 874-880, 1033-1039, 1-12, 109-121.

[23] Metthies, L., and Kanade, T., "Kalman Filter-based Algorithms for Estimating Depth from Image Sequences," *International Journal of Computer Vision,* Vol. 3, 1989, pp. 209-236.

[24] Kim, J., and Rock, S., "Stochastic Feedback Controller Design Considering the Dual Effect," *AIAA Guidance, Navigation, and Control Conference,* 2006.

[25] Frew, E.W., "Observer Trajectory Generation for Target-Motion Estimation Using Monocular Vision," Ph.D. Dissertation, Stanford University, August 2003.

[26] Kirk, D.E., "Optimal Control Theory, An Introduction," Dover, Mineola, NY, 2004.

[27] Bryson, A.E., Jr., and Ho, Y.C., "Applied Optimal Control," Hemisphere Publishing Corp., Washington D.C., 1975.

[28] Geiger, B.R., Horn, J.F., Sinsley, G.L., "Flight Testing a Real-Time Direct Collocation Path Planner," *Journal of Guidance, Control, and Dynamics,* Vol. 31, No. 6, 2008, pp. 1575-1586.

[29] Ross, J.A., Geiger, B.R., Sinsley, G.L., "Vision-Based Target Geolocation and Optimal Surveillance on an Unmanned Aerial Vehicle," *AIAA Guidance, Navigation and Control Conference and Exhibit,* 2008.

[30] Geiger, B.R., and Horn, J.F., "Neural Network Based Trajectory Optimization for Unmanned Aerial Vehicles," *47th AIAA Aerospace Sciences Meeting Including the New Horizons Forum and Aerospace Exposition,* American Institute of Aeronautics and Astronautics, 2009.

[31] Rysdyk, R., "UAV Path Following for Constant Line-of-Sight," *2nd AIAA Unmanned Unlimited Conference, Workshop, and Exhibit,* 2003.

[32] Wise, R., and Rysdyk, R.T., "UAV Coordination for Autonomous Target Tracking," *AIAA Guidance, Navigation and Control Conference and Exhibit,* 2006.

[33] Dobrokhodov, V.N., Kaminer, I.I., and Jones, K.D., "Vision-Based Tracking and Motion Estimation for Moving Targets Using Unmanned Air Vehicles," *Journal of Guidance, Control, and Dynamics,* Vol. 31, No. 4, July-August, 2008, pp. 907-917.

[34] Johnson, E.N., Calise, A.J., and Watanabe, Y., "Real-Time Vision-Based Relative Navigation," *AIAA Guidance, Navigation, and Control Conference,* 2006, pp. 4411-4456.

[35] Watanabe, Y., Johnson, E.N., and Calise, A.J., "Vision-Based Guidance Design from Sensor Trajectory Optimization," *AIAA Guidance, Navigation, and Control Exhibit,* 2006.

[36] Speyer, J., Hull, D., and Tseng, V., "Estimation Enhancement by Trajectory Modulation for Homing Missiles," *AIAA Journal of Guidance, Control, and Dynamics,* Vol. 7, No. 3, 1984.

[37] Hull, D., Speyer, J., and Burris, D., "Linear-Quadratic Guidance Law for Dual Control of Homing Missiles," *AIAA Journal of Guidance, Control, and Dynamics,* Vol. 13, No. 1, 1990.

[38] Hodgson, J.A., "Trajectory Optimization Using Differential Inclusion to Minimize Uncertainty in Target Location Estimation," *AIAA Guidance, Navigation, and Control Conference and Exhibit,* 2005.

[39] Watanabe, Y., Johnson, E.N., and Calise, A.J., "Stochastically Optimized Monocular Vision-Based Guidance Design," *AIAA Guidance, Navigation and Control Conference and Exhibit,* 2007.

[40] Watanabe, Y., Johnson, E.N., and Calise, A.J., "Stochastic Guidance Design for UAV Vision-Based Control Applications," *AIAA Guidance, Navigation, and Control Conference and Exhibit,* 2008.

[41] Cory, R., and Tedrake, R., "Experiments in Fixed-Wing UAV Perching," *Proceedings of the 2008 AIAA Guidance, Navigation, and Control Conference,* 2008.

[42] Taylor, J.H., "The Cramér-Rao Estimation Error Lower Bound Computation for Deterministic Nonlinear Systems," *IEEE Transactions on Automatic Control,* Vol. AC-24, No. 2, 1979, pp. 343-344.

[43] Ross, S. M., "Stochastic Real-Time Optimal Control: A Pseudospectral Approach for Bearing-Only Trajectory Optimization", PhD Dissertation, Air Force Institute of Technology, 2011.

[44] Ross, I.M., and Fahroo, F., "Issues in the Real-Time Computation of Optimal Control," *Mathematical and Computer Modeling,* Vol. 43, No. 9-10, 2006, pp. 1172-1188.

[45] Geiger, B.R., Horn, J.F., and DeLullo, A.M., "Optimal Path Planning of UAVs Using Direct Collocation with Nonlinear Programming," *AIAA Guidance, Navigation, and Control Conference Proceedings,* AIAA Paper 2006-6199, American Institute of Aeronautics and Astronautics, 2006.

[46] Williams, P., "Three-Dimensional Aircraft Terrain-Following via Real-Time Optimal Control," *Journal of Guidance, Control, and Dynamics,* Vol. 30, No. 4, 2007, pp. 1201-1205.

[47] Tsuchiya, T., Miwa, M., and Suzuki, S., "Real-Time Flight Trajectory Optimization and Its Verification in Flight," *Journal of Aircraft,* Vol. 46, No. 4, July-August 2009, pp. 1468-1470.

[48] Yan, H., "Pseudospectral Feedback Control for Three-Axis Magnetic Attitude Stabilization in Elliptic Orbits," *Journal of Guidance, Control, and Dynamics,* Vol. 30, No. 4, 2007, pp. 1107-1115.

[49] Betts, J.T., "Practical Methods for Optimal Control Using Nonlinear Programming," *Advances in Design and Control,* SIAM, Philadelphia, PA, 2001.

[50] Fornberg, B., "A Practical Guide to Pseudospectral Methods," Cambridge University Press, New York, NY, 1998.

[51] Fahroo, F., and Ross, I.M., "Direct Trajectory Optimization by a Chebyshev Pseudospectral Method," *Journal of Guidance, Control, and Dynamics,* Vol. 1, January-February 2002, pp. 160-166.

[52] Garg, D., Patterson, M., and Rao, A.V., "A Unified Framework for the Numerical Solution of Optimal Control Problems Using Pseudospectral Methods," *Automatica,* 2010, pp. 1-9.

[53] Garg, D., Patterson, M.A., and Darby, C.L., "Direct Trajectory Optimization and Costate Estimation of Finite-Horizon and Infinite-Horizon Optimal Control Problems Using a Radau Pseudospectral Method," *Computational Optimization and Applications,* 6 October 2009.

[54] Darby, C.L., Hager, W.W., and Rao, A.V., "An hp-Adaptive Pseudospectral Method for Solving Optimal Control Problems," *Optimal Control Applications and Methods,* Vol. 32, August, 2010.

[55] Brown, R.G., and Hwang, P.Y.C., "Introduction to Random Signals and Applied Kalman Filtering," John Wiley & Sons, New York, NY, 1997.

[56] Julier, S.J., and Uhlmann, J.K., "Unscented Filtering and Nonlinear Estimation," *Proceedings of the IEEE,* Vol. 92, No. 3, 2004, pp. 401-422.

[57] Ross, S.M., Cobb, R.G., and Baker, W.P., "Implementation Lessons and Pitfalls for Real-time Optimal Control with Stochastic Systems," *Optimal Control Applications and Methods,* Submitted for publication, September, 2010.

[58] Yan, H., "Real-time Computation of Neighboring Optimal Control Laws," *AIAA Guidance, Navigation, and Control Conference and Exhibit,* 2002.